QUARTERLY JOURNAL
OF THE
ROYAL METEOROLOGICAL SOCIETY

Vol. 125 APRIL 1999 Part A No. 555

Q. J. R. Meteorol. Soc. (1999), **125**, pp. 763–786

Maintenance of the African easterly jet

By C. D. THORNCROFT* and M. BLACKBURN
University of Reading, UK

(Received 6 November 1997; revised 21 May 1998)

SUMMARY

The maintenance of the African easterly jet (AEJ) has been examined using a zonally symmetric general circulation model with simple parametrizations. It is shown that the AEJ is maintained in association with two diabatically forced meridional circulations: one associated with surface fluxes and dry convection in the Saharan heat-low region and one associated with deep moist convection in the intertropical convergence zone equatorward of this. The heat-low heating, which reaches the height of the AEJ around 700 mb, is particularly important in maintaining the AEJ and its associated meridional gradients in potential vorticity. It is concluded that the mean observed AEJ results from a combination of the diabatically forced meridional circulations which maintain it and easterly waves which weaken it.

KEYWORDS: Convection Dynamics General circulation model Tropical atmosphere

1. INTRODUCTION

The African easterly jet (AEJ) is a midtropospheric jet located over tropical north Africa during the northern hemisphere summer. Figure 1 shows north–south cross-sections through the jet based on radiosonde data from Burpee (1972) and Reed *et al.* (1977). The AEJ can be seen as a prominent feature in the zonal wind, with a maximum of around 12.5 m s^{-1} at 600–700 mb and 15°N. The AEJ plays a crucial role in the west African monsoon system. The vertical shears associated with the jet are crucial in organizing moist convection and the generation of squall lines (e.g. Houze and Betts 1981); whereas the horizontal shears together with the vertical shears are important for the growth of easterly waves (e.g. Burpee 1972; Thorncroft and Hoskins 1994a and 1994b; Paradis *et al.* 1995). Also, in association with the marked interannual variability in seasonal rainfall in this region (e.g. Nicholson 1989), the AEJ has exhibited interannual differences (e.g. Newell and Kidson 1984, Fontaine *et al.* 1995). The role that these interannual differences in AEJ structure play in the growth of weather systems on the jet has yet to be determined (see Thorncroft and Rowell 1998). Despite the crucial role of the AEJ in determining the nature of the mesoscale and synoptic-scale weather systems in this region, the processes which maintain it have been rarely addressed.

Textbook explanations for the AEJ are usually based on the observed surface temperature gradient together with thermal wind balance. However, while this is consistent with the easterly shear, it does not explain why at around 700 mb the shear becomes westerly. The aim of this paper is to show that the AEJ is associated with two separate diabatically forced meridional circulations, one associated with dry convection in the Sahara and the other with deep moist convection in the intertropical convergence zone (ITCZ) equatorward of

* Corresponding author: Department of Meteorology, University of Reading, PO Box 239, 2 Earley Gate, Reading, Berkshire RG6 6BB, UK.

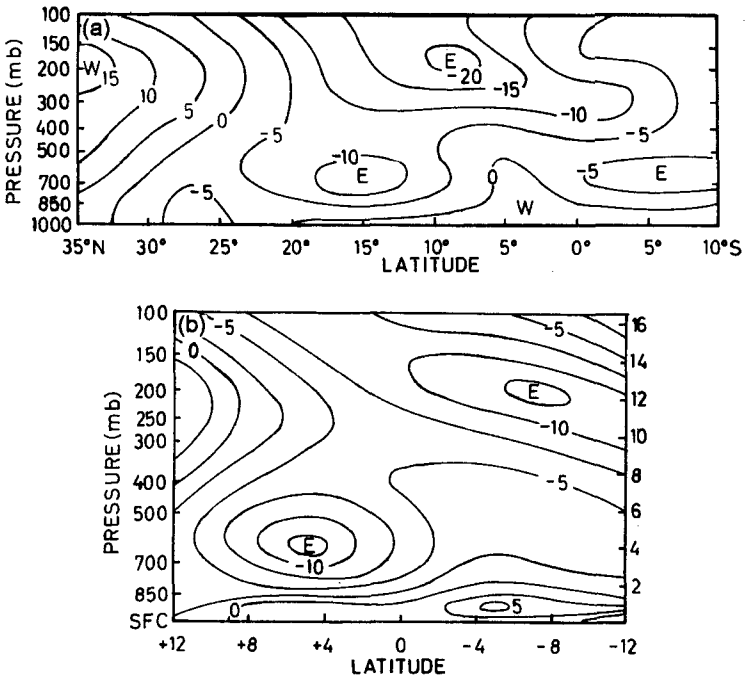

Figure 1. Mean zonal wind over north-west Africa from two observational studies: (a) the mean zonal wind for August at 5°E from Burpee (1972), contour interval 5 m s^{-1}; (b) the mean zonal wind during the GATE (Global Atmospheric Research Programme Atlantic Tropical Experiment) phase III period between 23 August and 19 September 1974 from Reed *et al.* (1977), contour interval 2.5 m s^{-1}. This is averaged between 10°E and 31°W; the 'zero' latitude corresponds to the average latitude of a disturbance path which was 11°N over land and 12°N over the ocean.

the Sahara. Although it was not the main purpose of their paper, Schubert *et al.* (1991; henceforward S91) emphasized the role of the ITCZ convection in maintaining the AEJ. To illustrate that the AEJ is in fact associated with the meridional variations in the type of convection, and cannot be explained by ITCZ convection alone, a schematic tephigram is shown in Fig. 2(a). Consider the surface temperature and humidity gradients present in the tropical north-west African region in summer. Typically the surface equatorward of 15°N is cooler and moister than that poleward of 15°N. At around 10°N the surface temperature and humidity are about 24 °C and 17 g Kg^{-1} respectively, whereas in the Saharan region around 25°N they are about 40 °C and nearer 7 g Kg^{-1}. Making the simple assumption that the mean temperature soundings in these two regions can be approximated by pseudo-adiabatic parcel ascent curves from the surface, we can see in Fig. 2(a) that the temperature soundings cross at about 700 mb. This implies that the positive meridional temperature gradient decreases with height in association with contrasting moist and dry adiabatic profiles in the equatorward and poleward regions respectively. From an examination of typical surface properties this simple construction predicts the height of the AEJ to be 700 mb in agreement with observations (cf. Fig. 1). From Fig. 2(a) it can be seen that the meridional temperature gradient changes sign in the mid-troposphere because the meridional gradient of surface equivalent potential temperature is negative.

To illustrate this further, Fig. 2(b) shows a mean temperature sounding based on radiosonde data from stations between about 5°N and 15°N for September for 11 years (Aspliden and Adefolalu 1976). Again, if we assume a surface temperature for the Saharan

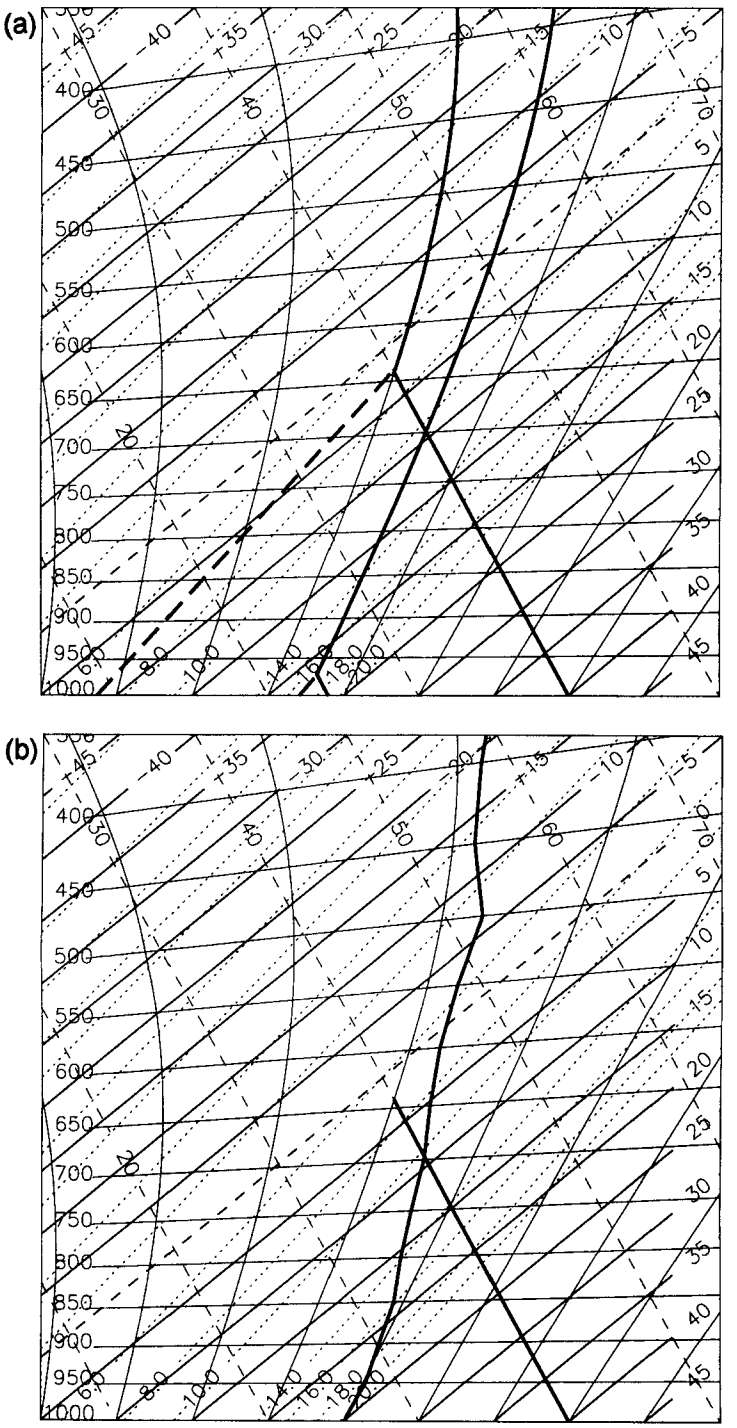

Figure 2. Tephigrams illustrating how the meridional temperature gradient decreases with height in the tropical north African region: (a) two pseudo-adiabatic parcel curves based on lifting low-level air parcels at around 10°N and 25°N; (b) the September mean temperature profile for west Africa taken from Aspliden and Adefolalu (1976) together with the 40 °C dry adiabat. See text for further details.

region of around 40 °C and low humidities, the AEJ height is predicted to be about 700 mb. One of the crucial components of this construction is the very deep well-mixed boundary layer in the Saharan region, which has been referred to in previous studies as the Saharan Air Layer (SAL; see Carlson and Prospero 1972 and Karyampudi and Carlson 1988).

An important focus of this study is the potential vorticity (PV) structure of the AEJ. This is because the AEJ is associated with distinctive PV anomalies and also because the associated meridional PV gradients are important in determining the nature of the mixed barotropic–baroclinic instability which gives rise to the African easterly waves (e.g. Thorncroft and Hoskins 1994a). Based on static-stability variations only, the idealised pseudo-adiabatic parcel curves in Fig. 2 trivially predict a negative meridional PV gradient in the lower troposphere. In S91 the authors were concerned mainly with the positive PV anomaly generated at low levels beneath the deep ITCZ heating. Here the role of the deep well-mixed zero-PV boundary layer to the north is also examined and shown to be an important feature of the AEJ. This feature of the west African climate has received very little attention, although Chang (1993) and Thorncroft (1995) have both considered the effect it would have on the African easterly waves.

The paper is organized as follows. In section 2 European Centre for Medium-Range Weather Forecasts (ECMWF) analyses are briefly examined to illustrate further the AEJ structure. After this, the paper is mainly concerned with an idealized modelling study of the AEJ using the spectral primitive-equation model of Hoskins and Simmons (1975). The model set-up is described in section 3. In section 4 the role of dry convection in forcing the AEJ is examined. In section 5 the role of the deep moist ITCZ convection (cf. S91) is also addressed, and in section 6, for completeness, the effect of having both the heat-low heating and the ITCZ heating together is briefly examined. A discussion and conclusions are presented in section 7.

2. ECMWF ANALYSES

The ideas introduced above suggest that an important role is played by the surface heating and dry convection in the Saharan region in the maintenance of the AEJ. There are few observations in the Sahara to aid our investigation of this. However, numerical weather prediction (NWP) analyses of this region are available. The aim of this section is to briefly examine the AEJ and its associated thermal structure in the ECMWF analyses, in the light of the discussion above. The PV structure will also be shown.

To illustrate the typically analysed AEJ structure, a meridional cross-section is presented in Fig. 3(a) of zonal wind averaged for a 16-day period in August 1995 and longitudinally averaged between 10°W and 10°E. The fields are averaged for 1200 UTC only, since this emphasises the dry convecting boundary layer which is most active during the daytime. The AEJ has a zonal wind maximum of 12.9 m s^{-1} located at around 600 mb and 15°N. Also evident in the section are the low-level monsoon westerlies beneath the AEJ with maxima equatorward and slightly poleward of the AEJ, together with the weaker low-level Harmattan easterlies poleward of the AEJ. Immediately above the low-level westerlies, near 200 mb, is the tropical easterly jet. Also seen is the subtropical westerly jet poleward of 20°N. All these features can be seen in the observed zonal wind distributions presented in Fig. 1.

The corresponding cross-section of potential temperature, θ, is shown in Fig. 3(b). The marked positive meridional θ-gradient below the AEJ is consistent with the marked easterly shear below the AEJ in Fig. 3(a). However, the most prominent feature is the deep well-mixed boundary layer poleward of 15°N, the height of which roughly coincides with the height of the AEJ. A weak sign reversal in the meridional θ-gradient above the AEJ

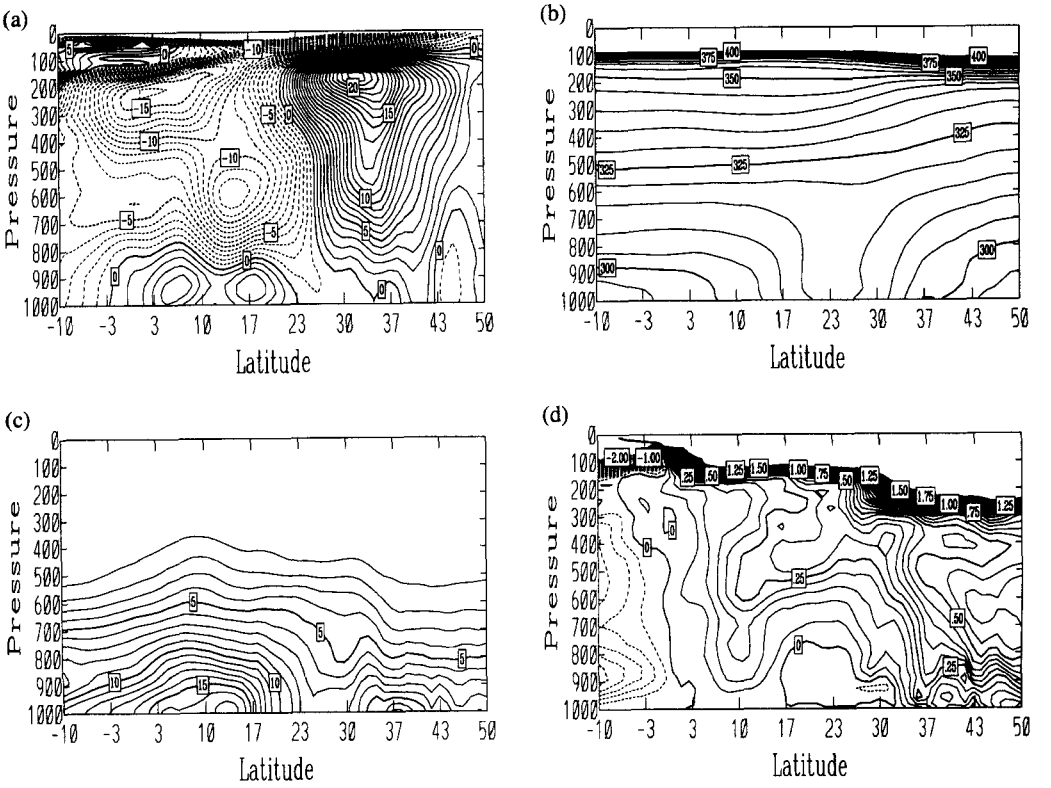

Figure 3. Latitude–pressure (mb) sections averaged between 10°W and 10°E over tropical north Africa, based on ECMWF analyses at 1200 UTC between 16 August and 31 August 1995. (a) Zonal wind, contour interval 1 m s^{-1} with dashed contours denoting easterlies; (b) potential temperature, contour interval 5 K; (c) specific humidity, contour interval 1 g kg^{-1}; (d) Ertel potential vorticity, contour interval 0.05 PV units (see Hoskins *et al.* 1985 for a discussion of PV units) with dashed contours denoting negative values.

is also evident, consistent with thermal wind balance. A comparison with other times of day (not shown) indicates a marked diurnal cycle in the analyses of low-level θ, with a marked deep well-mixed boundary layer at 1200 UTC and 1800 UTC and a shallow stable layer below the well-mixed layer at 0000 UTC and 0600 UTC.

For completeness, also shown in Fig. 3(c) is the corresponding section of specific humidity, q. As is well known, a marked meridional gradient in q exists with very low values in the region of the well-mixed boundary layer and much higher values around 12°N in the main deep-convection region.

Figure 3(d) shows the corresponding PV cross-section for this AEJ. The two most prominent PV features, as discussed above, are the positive midtropospheric PV anomaly near 11°N and the very low PV present in the lower troposphere between 17°N and 30°N. The marked negative meridional PV gradient present between these two regions, around 15°N and 600 mb, is coincident with the AEJ maximum. It is suggested here that the positive PV anomaly arises in association with ITCZ heating, consistent with the ideas discussed by S91, although there may be an advective contribution (see section 4), whereas the zero PV arises in association with the dry convective heating and the deep well-mixed boundary layer. These ideas will be investigated further with the model described in the next section.

Burpee (1972) also presented a zonal section of PV (not shown) based on the wind data shown here in Fig. 1(a). Although the resolution of the available data which were used to calculate the PV was very poor, Burpee's figure has very similar features to those seen in Fig. 3(d). One feature not obviously included in Burpee's figure is the deep well-mixed boundary layer, although this is almost certainly due to the lack of data over the Saharan region. Of course, the analyses shown here in Fig. 3 will suffer from the same deficiency, and we must recognise that much of the deep well-mixed boundary layer structure seen here will be model generated.

3. Model configuration

(*a*) *The model*

The spectral primitive-equation model of Hoskins and Simmons (1975) is used in a zonally symmetric configuration and with no moisture included. It has been integrated with 15 σ-levels at 0.033, 0.113, 0.216, 0.326, 0.432, 0.524, 0.600, 0.662, 0.714, 0.759, 0.803, 0.848, 0.894, 0.940 and 0.982. The horizontal spectral resolution has a truncation at wavenumber 95, giving a resolution equivalent to a half wavelength of about 210 km.

The model configuration is the same as that used in Thorncroft and Hoskins (1994b) except that in this study dry convection is included. The surface fluxes are parametrized using a bulk formulation with the stress convergence acting on the lowest three levels. It is acknowledged that this is a very simple representation of the tropical boundary layer, but it serves for an idealized investigation. The momentum and temperature forcings in the boundary layer (bl) are given by:

$$(\partial \mathbf{V}/\partial t)_{\mathrm{bl}} = -g/p_* \, \partial \boldsymbol{\tau}/\partial \sigma$$

$$c_p(\partial T/\partial t)_{\mathrm{bl}} = g/p_* \, \partial H/\partial \sigma,$$

where $\boldsymbol{\tau}$ and H are the stress and sensible-heat flux respectively, c_p is the specific heat capacity, p is pressure and a star denotes a surface value. At the surface $\boldsymbol{\tau}_* = C_{\mathrm{d}}\rho_*|\mathbf{V}'_{0.982}|\mathbf{V}_{0.982}$ where $|\mathbf{V}'_{0.982}|$ is the mean wind speed of the lowest model level including a constant 'gustiness factor' of 3.0 m s^{-1}, ρ is the density and C_{d} the drag coefficient. The forcings are prescribed to decrease linearly with decreasing σ, which is consistent with a quadratic vertical profile of $\boldsymbol{\tau}$ and H. A value for C_{d} of 4.0×10^{-3} has been used to be representative of the land. The bulk formulation for the heat flux is given by $H_* = \rho_* C_{\mathrm{h}}|\mathbf{V}'_{0.982}|\Delta\theta$, where $\Delta\theta$ is the potential-temperature difference between the surface and the lowest model level, and for simplicity we assume that the transfer coefficient C_{h} is equal to C_{d} and no stability or shear dependence is included.

Dry convection is parametrized by using a simple hard adjustment to a dry adiabat when the thermodynamic profile is dry unstable. Momentum is also mixed with a hard adjustment to the mean mass-weighted velocity of the unstable layer.

Following Lander and Hoskins (1997), a spectral filter is applied to the parametrized heating and momentum forcing as they are transformed from grid point to spectral space. This has the effect of suppressing forcing near the spectral truncation scale, which is poorly represented in the model. In practice the effects of the filter are largely cosmetic in the experiments described here, with minimal effect on the larger scales.

The sensitivity to important physical parameters is investigated in section 4(d).

(*b*) *Experimental approach*

Two types of zonally axisymmetric experiment will be presented here: (i) a heat-low run and (ii) an ITCZ run. The aim of the heat-low run is to isolate, as far as possible, the

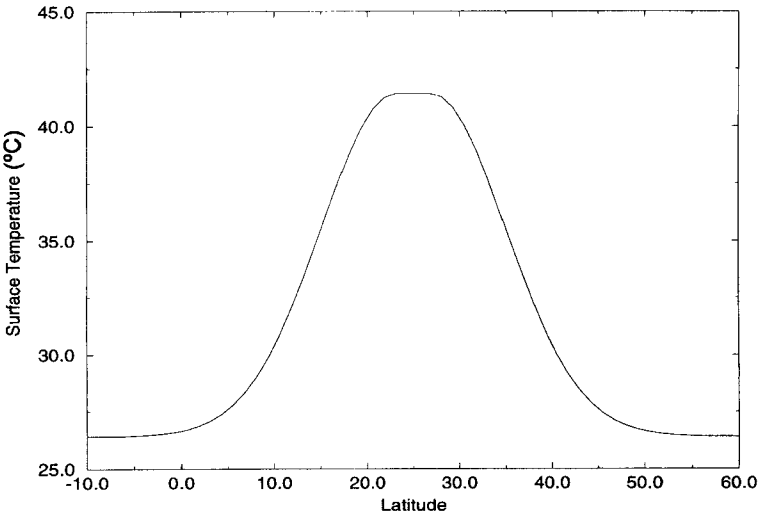

Figure 4. The prescribed surface temperature as a function of latitude used in the heat-low run (see text).

effects of the dry convection and the heat-low dynamics on the maintenance of the AEJ. The aim of the ITCZ run is to isolate the mechanism suggested by S91 for the maintenance of the AEJ. Both types of integration are initialized with a temperature profile based on that presented in Fig. 2(b) (see Simmons (1977) for details). The model is initialized globally with this profile and with zero winds. In both types of run, winds develop in response to the different types of heating.

It should be realized that the response we see in these simulations will be sensitive to the initial vertical temperature profile. For example, a colder profile will result in a deeper well-mixed boundary layer for the same prescribed surface temperature (cf. Fig. 2(b)). In order to avoid this arbitrariness, a more complete study should be considered using a more complex GCM which can develop its own radiative–convective equilibrium vertical temperature profiles. Since this will introduce more complications, and also because the aims of the present study can be met with a simple GCM without radiation or moist convection, this will be left to future work.

4. Heat-low run

(*a*) *Experimental design*

The heat-low run includes both the boundary layer and dry convection schemes. A meridional surface temperature profile is prescribed and kept fixed during the integration. The surface temperature profile shown in Fig. 4 has been chosen to give a typical temperature contrast of about 15 K between 23°N and 5°N (cf. Burpee 1972; Hastenrath 1991) and a maximum gradient at 15°N. For simplicity the profile is assumed to be symmetric, and thus has the same temperature gradient north of 30°N representing the contrast between the Mediterranean Sea and the Saharan desert region. Initially, in the region of the surface temperature maximum the surface is much warmer than the air above it, and so strong surface fluxes result, warming the lowest layers and subsequently leading to dry convection. Outside the region of the surface temperature gradients it has been arranged that the surface and lowest model-level have the same potential temperature, so that the

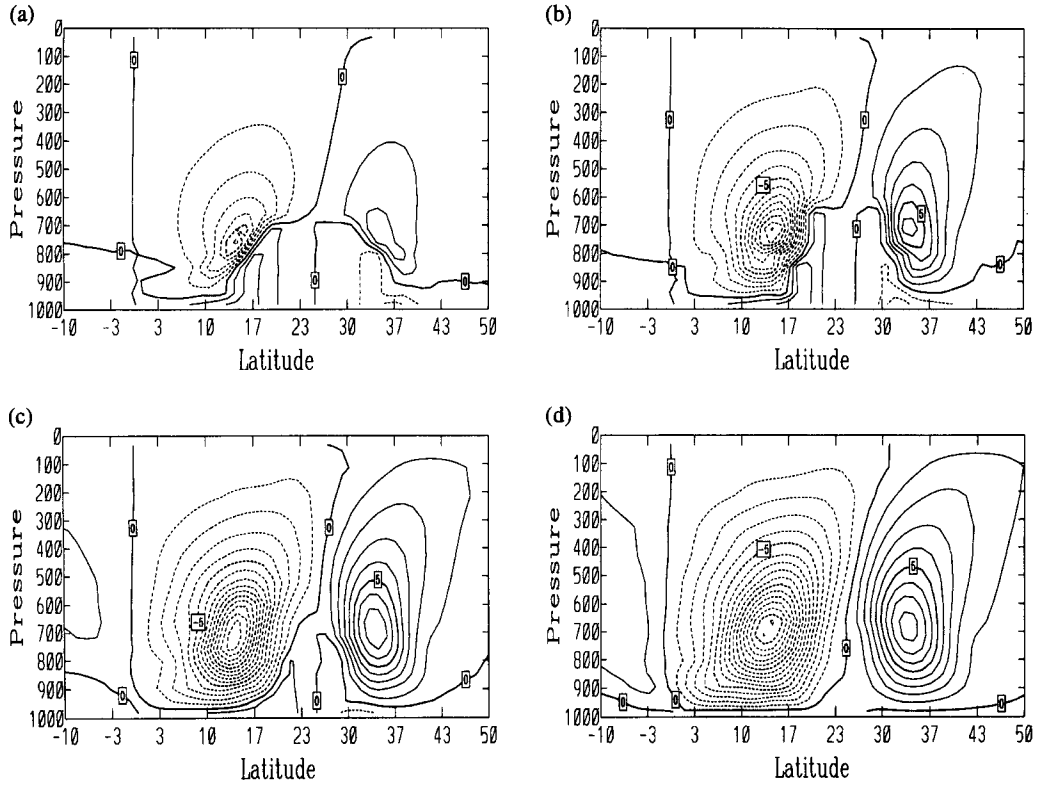

Figure 5. Latitude–pressure (mb) sections of zonal mean zonal wind at days: (a) 3, (b) 6, (c) 10 and (d) 20 in the heat-low run (see text); contour interval 1 m s^{-1} and dashed contours denote easterlies.

model boundary layer scheme is not activated; this means that all 'the action' in the model is restricted to the modelled heat-low region.

Based on the tephigram construction in Fig. 2 we would expect the AEJ to be located around 700 mb.

(*b*) *Results*

The heat-low run will be illustrated firstly by showing the zonal-wind distribution at days 3, 6, 10 and 20 (see Fig. 5). The model develops an AEJ, reaching a realistic amplitude of 11.1 m s^{-1} by day 6 (cf. Fig. 1). As expected the maximum is at a height of around 700 mb and a latitude of 15°N. Thus a realistic AEJ, with a sign reversal in the vertical shear, has been successfully forced using this idealized model, driven principally by differential surface heating and dry convection. Note that a midtropospheric westerly around 34°N also forms in response to this heating and the prescribed symmetric surface temperature profile (cf. Fig. 4), although with a weaker amplitude.

Figure 6 shows the magnitude of the midtropospheric easterly as a function of time. The graph indicates that by day 10 the AEJ has reached a quasi-steady-state amplitude, and so the zonal wind shown in Fig. 5(d) represents the steady-state structure reached by the model. It is interesting to note that the main difference between the day 20 state and, say, that at day 6 is the reduction in surface wind, suggesting that, although the transient response is characterized by surface winds, friction eventually weakens these in the longer

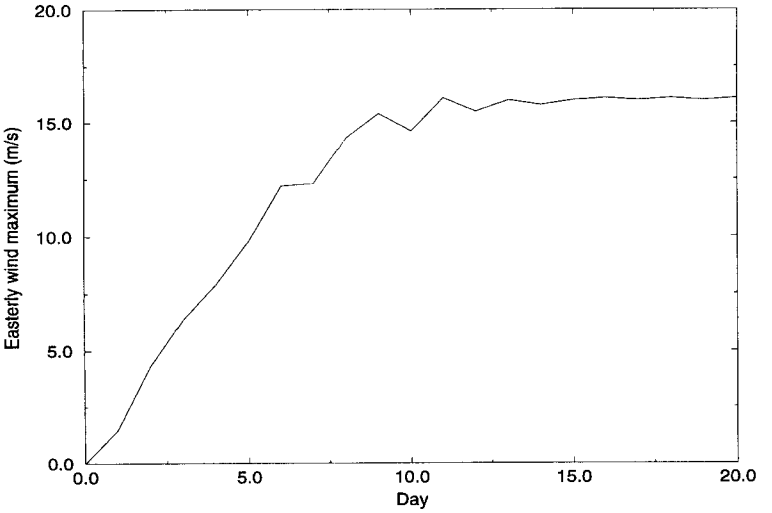

Figure 6. Time series of maximum easterly wind in the heat-low run (see text).

term. It should be realized, though, that this result does not mean that this steady state could be reached in reality. Easterly waves would be expected to develop before this and weaken the AEJ (cf. Thorncroft and Hoskins 1994b).

In order to illustrate how the AEJ develops in the model, time mean fields are presented averaged from day 0 to day 10, the spin-up period of the AEJ. The zonal wind and potential-temperature averages are shown in Figs. 7(a) and (b). Note again the midtropospheric easterly and westerly jets as well as surface westerlies and easterlies, equatorward and poleward respectively, of the surface temperature maximum (cf. Fig. 3(a)). Note also the deep dry convective boundary layer, characterized by vertically orientated isentropes in Fig. 7(b) and vertically orientated zonal wind contours in Fig. 7(a).

The mean heating associated with the dry convection and surface fluxes is shown in Fig. 7(c). A dome of positive heating rates is indicated over the Saharan region reaching a maximum height of about 700 mb near 26°N and sloping downwards, poleward and equatorward of this. This heating is a combination of that associated with the dry convection, which takes place at the beginning of the model integration, and the subsequent heating which is influenced by the circulation and associated heat fluxes which develop in response to that heating. The mean meridional circulation is shown in Fig. 7(d). As in previous studies based on zonally symmetric heating in equatorial regions (e.g. Gill 1982; Lindzen and Hou 1988 and Hack *et al.* 1989), two overturning cells result, with a stronger and more meridionally extensive cell on the equatorward side. As discussed in these previous studies, the asymmetry arises because of the weaker value of the Coriolis parameter on the equatorward side. Included in Figs. 7(d) and (e) are the corresponding mean vertical velocity and mean meridional wind which, consistent with Fig. 7(d), have larger magnitudes on the equatorward side of the heat-low. Interestingly, the meridional cells are concentrated at the edges of the heat-low where the surface temperature gradients are most marked, resulting in ascending regions which are clearly separated on either side of the heat-low.

We can therefore see that, as in the case of modelled Hadley circulations forced by imposed deep heating, the zonal jets in the present study form in association with the

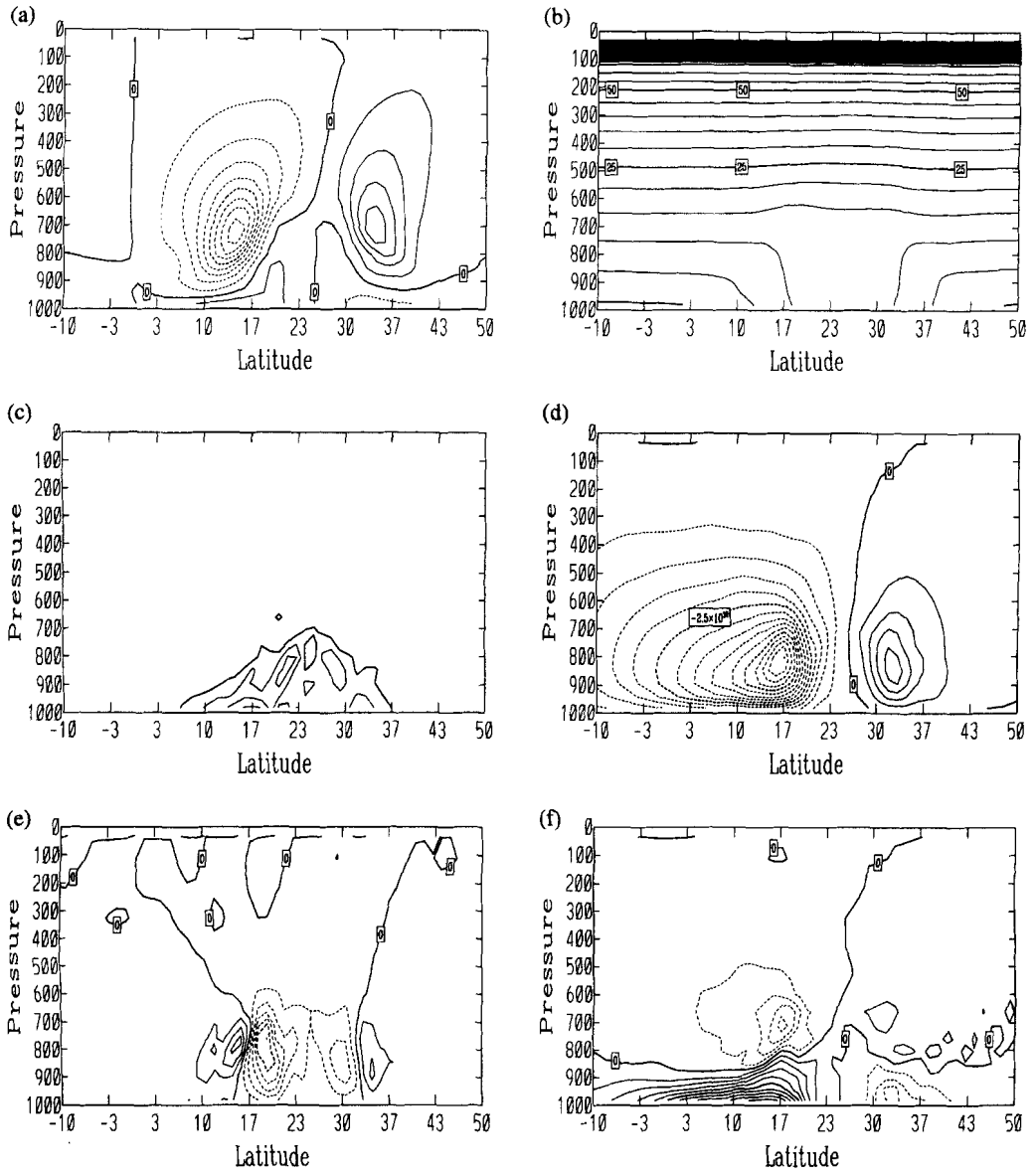

Figure 7. Latitude–pressure (mb) sections of day 0 to day 10 averaged zonal mean fields from the heat-low run (see text). (a) Zonal wind, contour interval 1 m s^{-1} with dashed contours denoting easterlies; (b) potential temperature minus 300 K, contour interval 5 K; (c) diabatic heating, contour interval 0.5 K day^{-1}; (d) meridional circulation, contour interval 0.5 × 10^{10} kg s^{-1}; (e) vertical velocity, contour interval 0.2 Pa s^{-1} with dashed lines denoting ascent; (f) meridional wind, contour interval 0.2 m s^{-1} with dashed contours denoting northerlies.

meridional overturning cells which are the adiabatic response to the model heating. For example, the AEJ near 15°N and 700 mb, forms through angular momentum conservation in the equatorward moving branch of the cell on the equatorward side of the heat-low (cf. Figs. 7(a) and (d)). The meridional circulation through maintaining a state close to thermal wind balance, does not only provide easterly acceleration in the midtroposphere. Through adiabatic cooling in the rising branch and adiabatic warming in the sinking branch above the level of the diabatic heating, it also provides the negative meridional temperature gradient

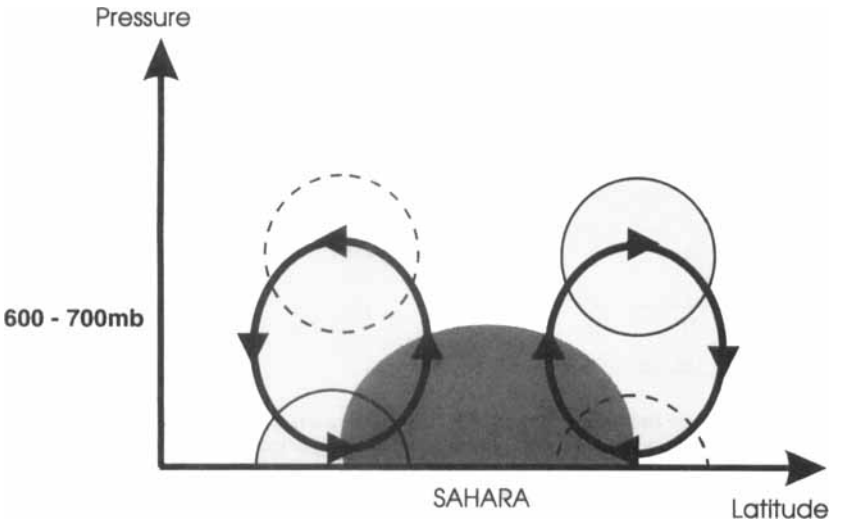

Figure 8. A schematic illustrating the response in the wind field to deep sensible heating in the Saharan region. The shading indicates the domed heating region, and the thick solid lines with arrowheads show the resulting meridional circulation which forms at the northern and southern fringes of the desert as a response to this heating. Through conservation of angular momentum, the poleward and equatorward branches of these overturning cells result in westerly (denoted by the thin solid lines) and easterly (denoted by the dashed lines) acceleration, respectively. The ascending branches of the overturning cells 'overshoot' the region of heating, resulting in the adiabatic cooling necessary for maintaining thermal-wind balance above the AEJ maximum at around 600–700 mb.

consistent with a reversal in the zonal wind shear. The situation is shown schematically in Fig. 8, which indicates rising motion in the region of heating. However the rising branches of the cells overshoot the heating region, resulting in adiabatic cooling there. The result of this can be seen clearly in Fig. 7(b) as a bulge in the isentropes. Low-level zonal winds also form in association with the low-level branches of the overturning cells, with surface westerlies apparent below the AEJ. Identical processes of opposite sign occur on the poleward side of the surface temperature maximum. It is noticeable that most of the low-level and midtropospheric features seen in the ECMWF analyses (Figs. 3(a) and (b)), are evident in this experiment.

The results show that, as in the case of all zonal jets which form as a response to heating, the easterlies of the AEJ form in association with the northerly branch of an overturning cell. A meridional temperature gradient above the AEJ forms in association with adiabatic cooling and warming, consistent with a sign reversal in the vertical shear. In this simulation the meridional circulation is strongest at the beginning of the integration, and weakens after this as the AEJ essentially reaches a balanced state. In reality this steady state may not be reached due to the modification by easterly-wave activity (not present here), and hence a meridional circulation will be maintained.

(*c*) *Potential vorticity*

As discussed in S91 the PV structure of the AEJ is of particular interest since the meridional PV gradients are important in determining the nature of the mixed barotropic–baroclinic instability which is important for easterly-wave growth (Burpee 1972). Indeed S91 suggested that the negative meridional PV gradients observed in the AEJ region arise in association with the diabatically generated positive PV anomaly from the deep ITCZ heating alone (see section 5 below). The 0 to 10-day average PV from the present run is

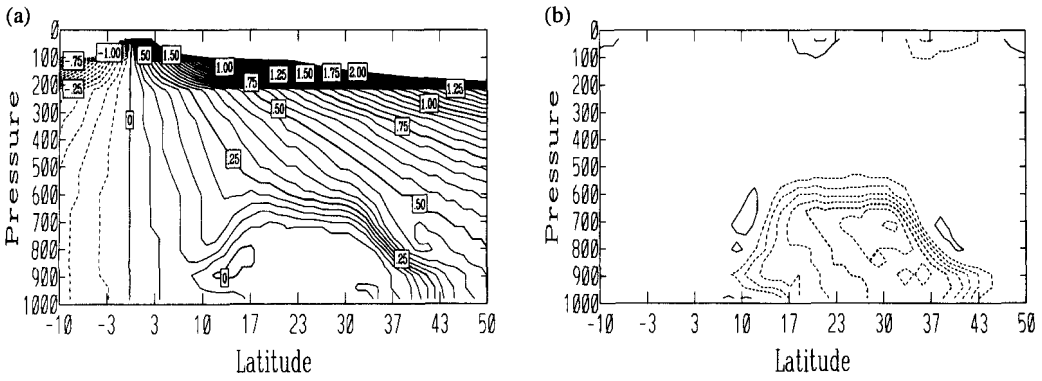

Figure 9. Latitude–pressure (mb) sections of (a) day 0 to day 10 averaged zonal mean PV from the heat-low run (see text), contour interval 0.05 PV units with dashed lines denoting negative values; (b) day 10 minus day 0 PV from the same run, contour interval 0.05 PV units with dashed contours denoting PV reduction over the 10-day period.

shown in Fig. 9(a) and is characterized by very small PV values in the region of the well-mixed boundary layer, as expected, and in agreement with the ECMWF analyses above (cf. Fig. 3(d)). Indeed the domed boundary layer is easily seen with marked PV gradients above it. Marked meridional PV gradients also result. Note in particular, the meridional contrast in PV around 700 mb between the relatively high PV at 11°N and the much lower PV in the region poleward of this. This negative meridional PV gradient is particularly important since, together with the positive meridional PV gradient on the equatorward side of the PV maximum at 11°N, the necessary Charney–Stern (1962) instability condition is satisfied. The necessary condition for baroclinic instability is also satisfied, since this negative meridional PV gradient has the opposite sign to the meridional surface temperature gradient (see Thorncroft and Hoskins 1994a). Note that the positive meridional PV gradients on the poleward side of the heat-low are larger than on the equatorward side. This is because the zero-PV boundary layer grows into a region of initially positive PV gradient, dominated by the planetary vorticity gradient, resulting in greater contrast on the poleward side. There is also some indication of this in Fig. 3(d).

Although it is suggested here that the negative meridional PV gradient arises mainly in association with the intrusion of the zero-PV boundary layer, the contrast is further enhanced through some equatorward and downward advection of relatively high PV on the equatorward side of the AEJ, in association with the descending branch of the overturning cell. This is indicated in Fig. 9(b) which shows the difference between the PV at day 10 and at day 0. The largest negative anomaly has a magnitude of 0.36 PV units (see Hoskins *et al.* 1985 for a discussion of PV units) on the poleward side of the heat-low as expected. The positive anomaly on the equatorward side of the heat-low has a much smaller magnitude of around 0.05 PV units. The anomalies seen above 100 mb, and also in Figs. 14 and 16, are associated with weak vertical velocities which develop there in association with gravity wave activity and are insignificant when compared with the ambient values there of greater than 10 PV units.

(*d*) *Sensitivity experiments*

In order to test the robustness of the results presented in section 4(b) above, the sensitivity of the AEJ to changes in physical parameters has been examined. The parameters

TABLE 1. SUMMARY OF HEAT-LOW SENSITIVITY EXPERIMENTS SHOWING THE STRENGTH OF THE AEJ AT DAY 20 AND WHEN IT REACHED 10 m s^{-1}.

Parameters changed from those in the basic heat-low run and their new values	Description of experiment	Day 20 easterly max (m s^{-1})	Time when easterly reached 10 m s^{-1} (days)
	Basic heat-low run presented in section 4(b)	16.1	5.1
$C_d = C_h = 0.002$	Weaker boundary layer	15.1	7.0
$C_d = C_h = 0.008$	Stronger boundary layer	16.0	3.6
$C_h = 0.008$	Stronger heat fluxes	16.5	3.6
$C_d = 0.008$	Stronger momentum fluxes	15.5	5.7
$\sigma_{bl} = 0.826$	Deeper boundary layer	15.4	4.5
$\sigma_{bl} = 0.917$	Shallower boundary layer	15.4	4.8
$T_{dc} = 2$ hours	Weaker dry convection	15.7	5.0

investigated are: the transfer coefficients C_d and C_h, which determine the surface momentum and heat fluxes respectively; the depth of the boundary layer, σ_{bl} and the time-scale for dry convective adjustment, T_{dc}. For reference, the heat-low run described above had the following parameters: $C_d = C_h = 0.004$, $\sigma_{bl} = 0.871$ and $T_{dc} = 0.5$ hours. The different experiments are summarized in Table 1.

An AEJ develops in all of the experiments. As in the control run, most of the AEJ development occurs up to about day 10, after which a quasi-steady state is reached. The AEJ structures that develop in all the experiments are very similar to those presented in the basic heat-low run above (not shown). The small differences can be appreciated by an examination of Table 1, which includes the AEJ magnitude at day 20 together with the time when the AEJ reached 10 m s^{-1}. The magnitude of the AEJ at day 20 in all the experiments is very similar ranging between 15.4 and 16.1 m s^{-1}, suggesting that for the range of parameters examined here the steady state AEJ is fairly insensitive. The same is not true, however, for the rate at which the AEJ develops. Table 1 shows that the time for an AEJ to develop an easterly with a magnitude of 10 m s^{-1} is shorter by 1.5 days when C_h is doubled, whereas when C_d is doubled it takes 0.6 days longer. When both C_d and C_h are changed together it appears that the rate of development is determined more by the value of C_h than of C_d (cf. Table 1). The rate of AEJ development appears relatively insensitive to the boundary layer depth and the time-scale for dry convection, for the ranges examined here.

It is concluded from this that the mechanism for AEJ development discussed in section 4(c) is robust. A very similar AEJ development occurs in all of the experiments examined. For the parameters varied here the greatest sensitivity was found in the time-scale for the AEJ development, and this was found to be most sensitive to changes in C_h. Unlike reality, an AEJ develops in these experiments from an initial state with no zonal winds. In reality the AEJ will be weakened by growing easterly waves but not removed (cf. Thorncroft and Hoskins 1994b); thus it is envisaged that similar processes to those seen in these experiments will occur to replenish the AEJ and maintain it. These results suggest that the rate at which the AEJ is replenished in numerical models could be sensitive to *how* the surface fluxes are parametrized.

(*e*) *Summary*

A realistic AEJ has been produced in this idealized model which emphasises the role of dry convection and the associated deep well-mixed boundary layer over the Sahara. The AEJ forms in association with a diabatically forced meridional cell on the equatorward side of the heat-low. In contrast to S91, the negative meridional PV gradient is produced in association with the zero-PV boundary layer and the induced meridional circulation advecting relatively high PV equatorwards and downwards on the equatorward side of the AEJ. This view of the AEJ, and in particular the formation of the negative meridional PV gradient, contrasts with the conceptual model proposed by S91. It is likely, however, that the ITCZ heating mechanism proposed in that study also operates in the African region together with the heat-low forcing. Similar ITCZ heating experiments to those shown in S91 are therefore repeated in the next section for comparison with the heat-low experiment, and are combined with the heat-low in section 6.

5. ITCZ HEATING RUNS

(*a*) *Experimental design*

The ITCZ heating runs are based on those presented in S91. As in that study, a fixed heating rate is prescribed in the thermodynamic equation to mimic the heating effect of deep moist convection in the ITCZ region around 10°N. As in S91, the vertical and horizontal structure are prescribed. S91 used a model with potential temperature as the vertical coordinate, and used vertical sine and sine^2 profiles based on potential temperature. Here we also use sine and sine^2 profiles but based on the model σ coordinate. The two heating-rate profiles are given by:

$$Q(\phi, \sigma) = Q_0 \sin\{\pi(\sigma - 0.1)/(0.9)\} \exp -[\{(\phi - \phi_0)/\Delta_\phi\}^2]$$

$$Q(\phi, \sigma) = Q_0 \sin^2\{\pi(\sigma - 0.1)/(0.9)\} \exp -[\{(\phi - \phi_0)/\Delta_\phi\}^2],$$

where σ is the height variable, ϕ is the latitude in degrees, Q_0 is a heating-rate amplitude, ϕ_0 is the latitude of maximum heating rate, and Δ_ϕ determines the latitudinal width of the heating. Here $Q_0 = 5$ K day^{-1}, $\Delta_\phi = 3°$ and $\phi_0 = 10°$N. The two heating-rate distributions are shown in Figs. 10(a) and (b).

Since the PV generated by such heating is proportional to the vertical gradient of the heating rate (cf. Hoskins *et al.* 1985), S91 suggested that the sine^2 profile could account for the observed midtropospheric AEJ. This is because the maximum vertical gradient of the sine^2 profile is elevated, whereas the maximum vertical gradient of the sine profile is at the surface. It is suggested here that the sine profile is more realistic (e.g. see Yanai *et al.* 1973; Betts and Miller 1986), and that another reason for the elevated AEJ which forms in association with ITCZ heating alone could be associated with surface friction reducing the winds at low levels. In this section, three ITCZ heating experiments are examined: one using the sine^2 heating profile, one using the sine heating profile, and one using the sine heating profile but with the boundary layer included. These will be referred to as the sine^2, sine and sine-BL runs respectively.

(*b*) *Results*

Included in Fig. 10 for comparison with S91 are the zonal wind distributions at day 6 for the sine and sine^2 runs (cf. S91 Fig. 3 and Fig. 6). As for the heat-low runs, diabatically forced meridional cells result in zonal jets. Despite the difference in the model formulation (S91 used a PV-balance model) the jet structures and their magnitudes are very similar.

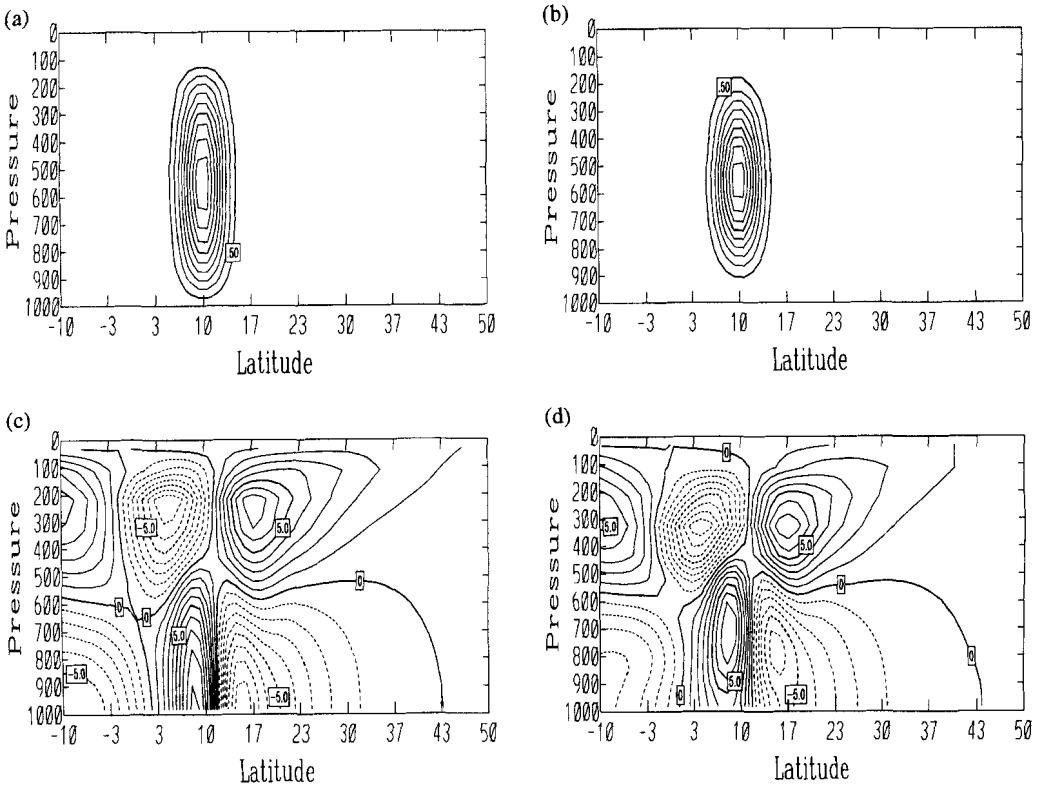

Figure 10. Latitude–pressure (mb) sections of the prescribed ITCZ diabatic heating distributions used in (a) the sine run and (b) the sine^2 run, contour interval 0.5 K day^{-1}, and the zonal mean zonal wind at day 6 in (c) the sine run and (d) the sine^2 run, contour interval 1 m s^{-1} with dashed contours denoting easterlies. See text for further details.

For comparison with the 0 to 10-day averages presented above in the case of the heat-low runs, Figs. 11 and 12 show 0 to 10-day averaged fields for the sine and sine^2 cases respectively. In agreement with S91, the jets that form below the heating maximum form at the surface with the sine profile but are elevated with the sine^2 profile. Focussing on the lower-tropospheric easterly jet which forms, in the sine case the jet is located around 15°N at the ground and has a magnitude of about 7 m s^{-1}, whereas in the sine^2 case it is located at 15°N at a height of around 800 mb and has a magnitude of about 5 m s^{-1}. Note that, unlike the case of the heat-low runs or in the ECMWF analyses, the meridional temperature gradients which develop are very weak.

S91 suggested that the easterly jet below and poleward of the sine^2 heating maximum can be related to the AEJ, and that the AEJ can be explained by ITCZ convection alone with no need to invoke surface heating. The results from the present study (cf. section 4) lead us to suggest that, although ITCZ convection alone can result in an easterly jet, the dry convection in the heat-low plays a crucial role in AEJ maintenance. In fact the heat-low heating alone leads to a more realistic AEJ structure and magnitude than the ITCZ heating alone. Also, the ITCZ heating produces a jet pair, with a stronger westerly jet equatorward of the easterly, which is not observed.

Included in Figs. 11 and 12 are the corresponding mean vertical and meridional velocities. As before, the meridional circulation is characterized by asymmetric overturning

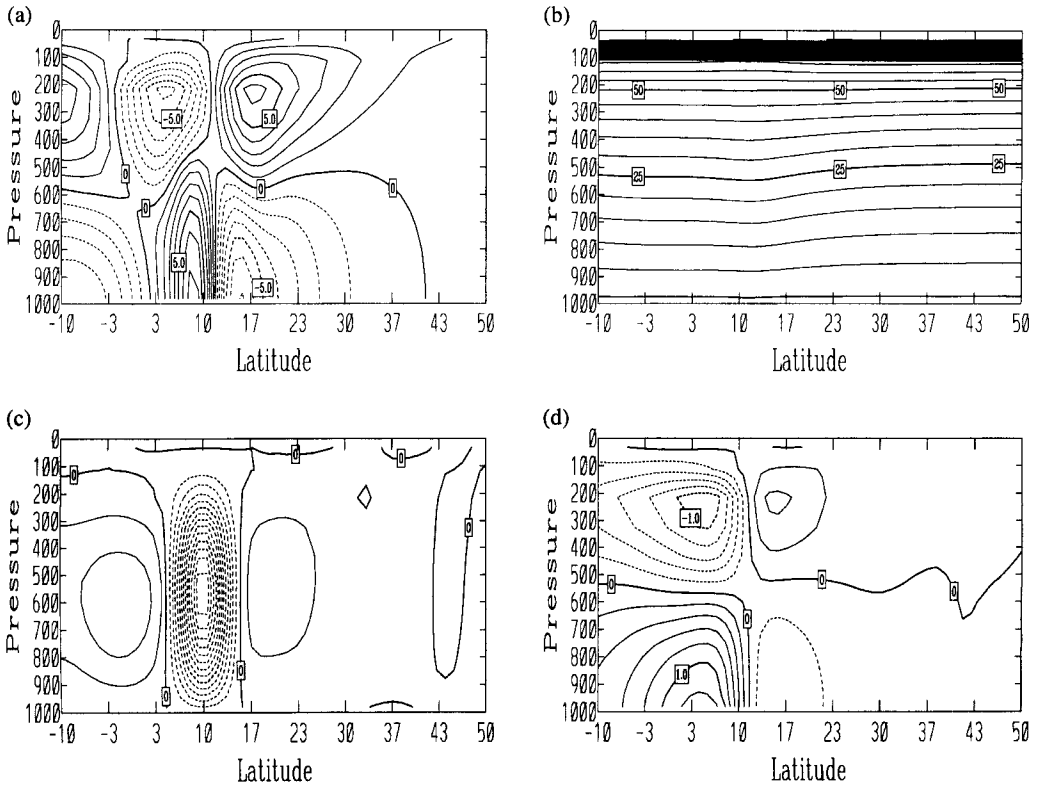

Figure 11. Latitude–pressure (mb) sections of day 0 to day 10 averaged zonal mean fields from the ITCZ sine run (see text). (a) Zonal wind, contour interval 1 m s^{-1} with dashed contours denoting easterlies; (b) potential temperature minus 300 K, contour interval 5 K; (c) vertical velocity, contour interval 0.2 Pa s^{-1} with dashed lines denoting ascent; (d) meridional wind, contour interval 0.2 m s^{-1} with dashed contours denoting northerlies.

cells. It is worth noting, however, the unrealistic depth of the low-level southerly inflow. In reality, the overturning and heating are mutually consistent, with southerly inflow supplying moisture to maintain deep moist convection, whereas here the inflow forms as a response to the prescribed heating. In reality, the moist inflow layer reaches a maximum height of about 850 mb, whereas in the sine case it reaches 600 mb and in the $\sin e^2$ case it actually peaks above 850 mb. Clearly there is some inconsistency in these results. This arises because of the idealized heating profiles used and the generally idealized nature of these experiments; for example, no account is taken of an oceanic trade-wind boundary layer with a capping inversion which, in reality, is likely to limit the depth of the inflow layer. With the knowledge that the inflow layer only reaches 850 mb it is trivial to construct a heating profile which is more consistent with this. This profile is characterized by strong vertical heating gradients at low levels only. An experiment with such a heating profile (not shown) does indeed produce a more shallow inflow.

It was suggested above that including a frictional boundary layer would result in elevated jets, even when using the more realistic sine heating profile. With this in mind, the sine run was repeated with the simple boundary layer representation described in section 3. The resulting 0 to 10-day average fields are shown in Fig. 13. Note that, as expected, the easterly wind maximum which forms below the heating maximum is now elevated, and has a maximum of 3.4 m s^{-1} at about 800 mb. Note also that the inclusion

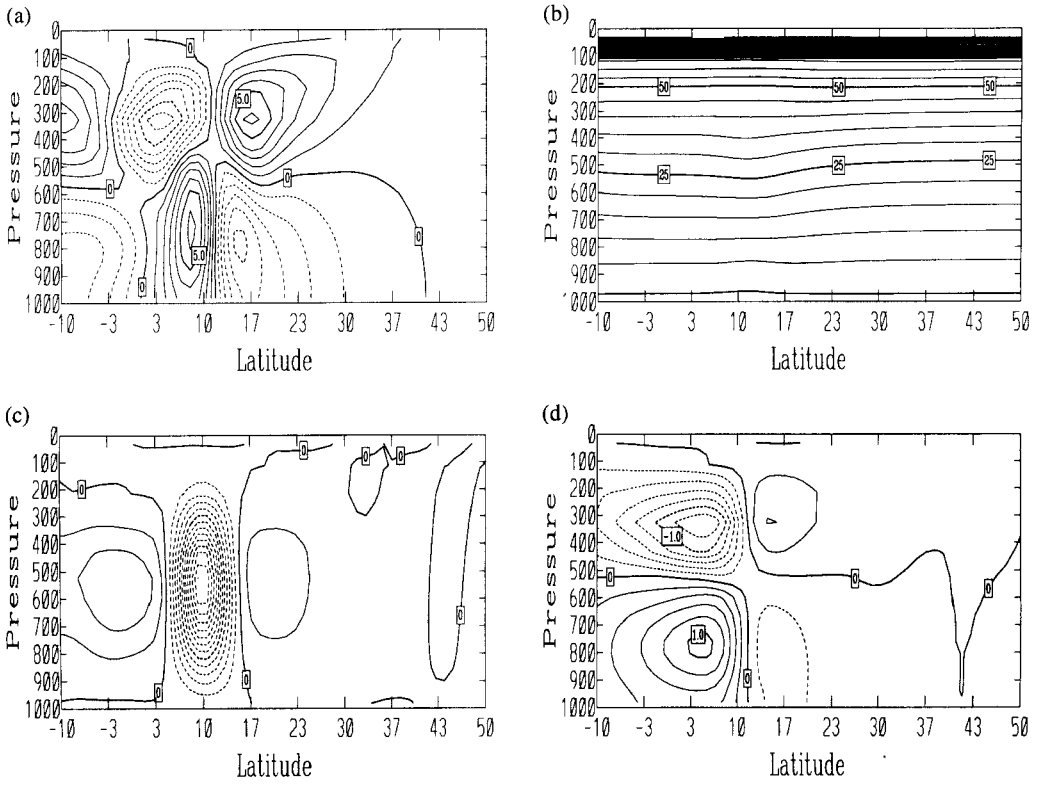

Figure 12. As Fig. 11 but for the sine^2 run.

of the boundary layer tends to concentrate the inflow a little lower down than before and makes it slightly stronger. This is associated with the fact that the zonal wind without the boundary layer is stronger than the meridional wind (cf. Fig. 11(a) and (d)) and therefore the friction acts most strongly on the zonal component of the wind. The deceleration of the low-level easterly wind enhances the low-level northerlies in the region of the easterly jet. From these results it is concluded that the tropospheric winds which form in response to heating can be substantially modified by boundary layer processes, which should therefore be included, even when considering only ITCZ heating.

(*c*) *Potential vorticity*

The 0 to 10-day averaged PV distributions for the sine, sine^2 and sine-BL runs are shown in Fig. 14 together with the corresponding day 10 minus day 0 differences. Consistent with the wind distribution in Fig. 11(a), a PV maximum is generated at the ground in the sine run. Note also that, consistent with the generation of positive PV in a background state with positive meridional PV gradient, the meridional PV gradients are largest and positive on the equatorward flank of the anomaly. Negative and positive PV anomalies also result above the heating associated with the heating and vertical advection respectively, resulting in a marked negative PV gradient there. The PV distribution in the sine^2 run shows an elevated PV maximum at around 700 mb consistent with the heating profile. Again, the positive meridional PV gradient on the equatorward flank of the anomaly is most prominent. Finally, the PV distribution for the sine-BL run indicates an elevated PV

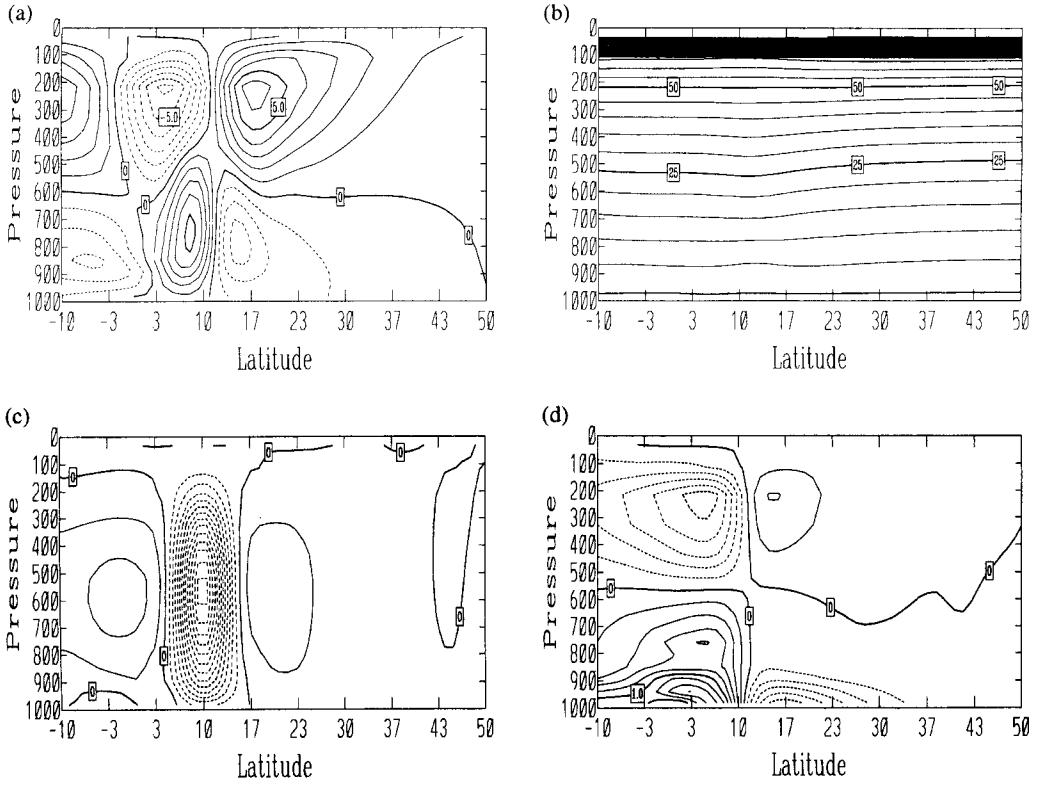

Figure 13. As Fig. 11 but for the sine-BL run.

maximum. Thus, although the heating in this case generates highest PV at the surface, friction acting most strongly at the surface erodes this, resulting in a PV maximum at around 800 mb. It should be noted that friction does not always act to decrease the PV. As discussed in Cooper *et al.* (1992), if the surface wind opposes the thermal wind, surface friction will act to increase the low-level PV by decreasing the horizontal component of vorticity. In the present case this effect is negligible, consistent with weak vertical shear, and the change in PV is dominated by a decrease in low-level cyclonic vorticity.

(d) Summary

Idealized sine and sine^2 heating profiles have been used here to produce zonal jets similar to those seen in S91. The asymmetric deep overturning Hadley cells result in upper-level and low-level zonal jets. The upper-level northerly of the equatorward cell results in an upper-level tropical easterly jet consistent with observations (cf. Fig. 1). Similarly, the low-level northerly of the weaker poleward cell results in a low-level easterly which S91 related to the AEJ. The sine heating profile results in a surface easterly which bears little resemblence to the observed elevated AEJ. An elevated AEJ can only be obtained with a less realistic sine^2 heating profile as in S91, or as suggested here, by including boundary layer friction. To further our understanding of the role of deep heating in the maintenance of the AEJ we need to know more about the vertical heating profiles in the region. Alongside this, further work is required on the role of surface processes and in particular their effects on the PV distribution.

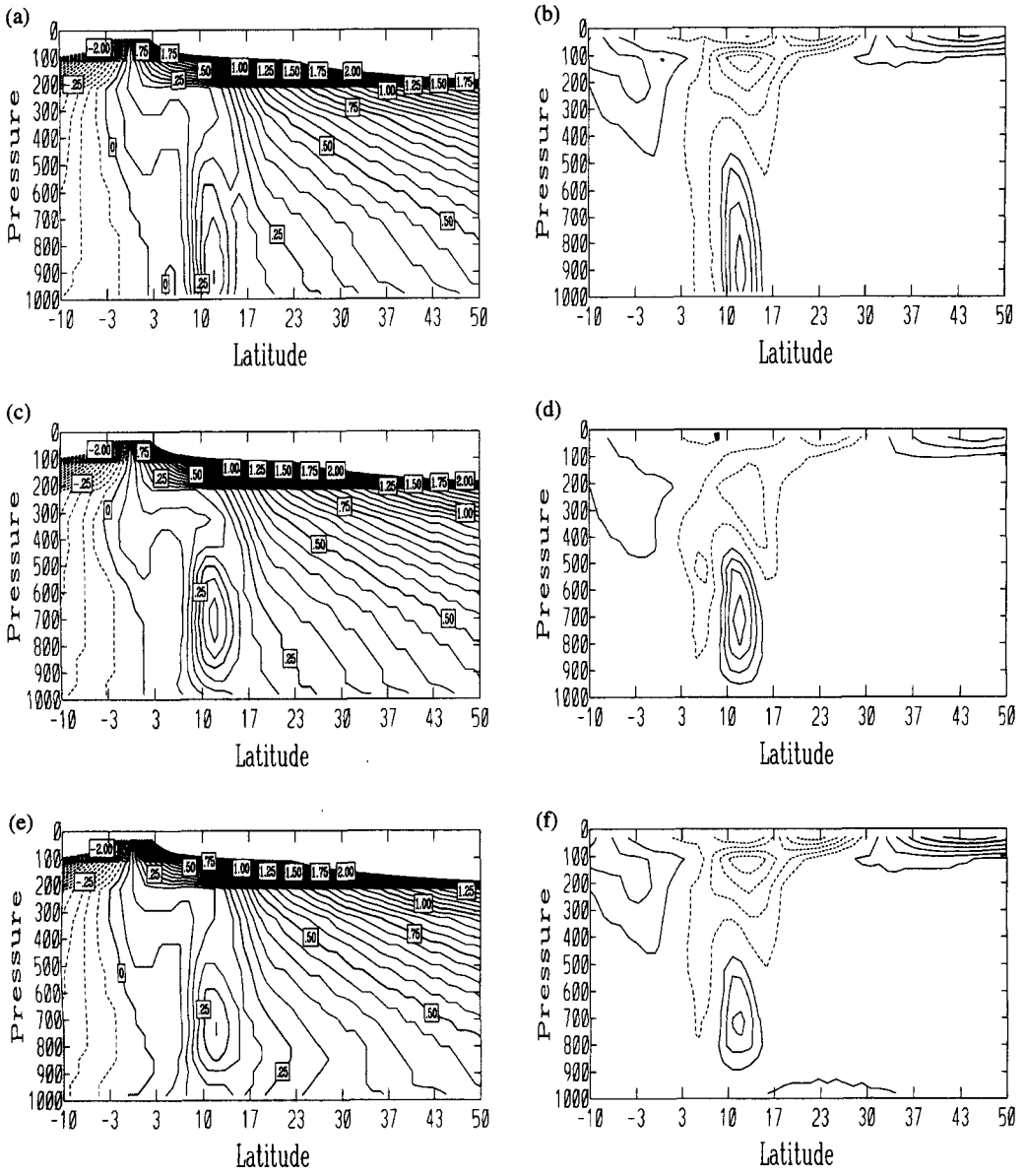

Figure 14. Latitude–pressure (mb) sections of day 0 to day 10 averaged zonal mean PV from (a) the ITCZ sine run, (c) the ITCZ sine^2 run and (e) the ITCZ sine-BL run, contour interval 0.05 PV units with dashed lines denoting negative values. Also latitude–pressure (mb) sections of day 10 minus day 0 PV from (b) the ITCZ sine run, (d) the ITCZ sine^2 run and (f) the ITCZ sine-BL run, contour interval 0.05 PV units with dashed contours denoting PV reduction over the 10-day period. See text for further details.

Since the deep heating produces a positive lower-tropospheric PV anomaly in a background state which has a positive meridional PV gradient, it results in more pronounced positive than negative meridional lower-tropospheric PV gradients. This is in contrast to the heat-low heating, which creates a negative PV anomaly in the same background initial state, resulting in a more prominent negative meridional PV gradient in the AEJ region. It is suggested here that since, in reality, we expect the ITCZ heating to occur together

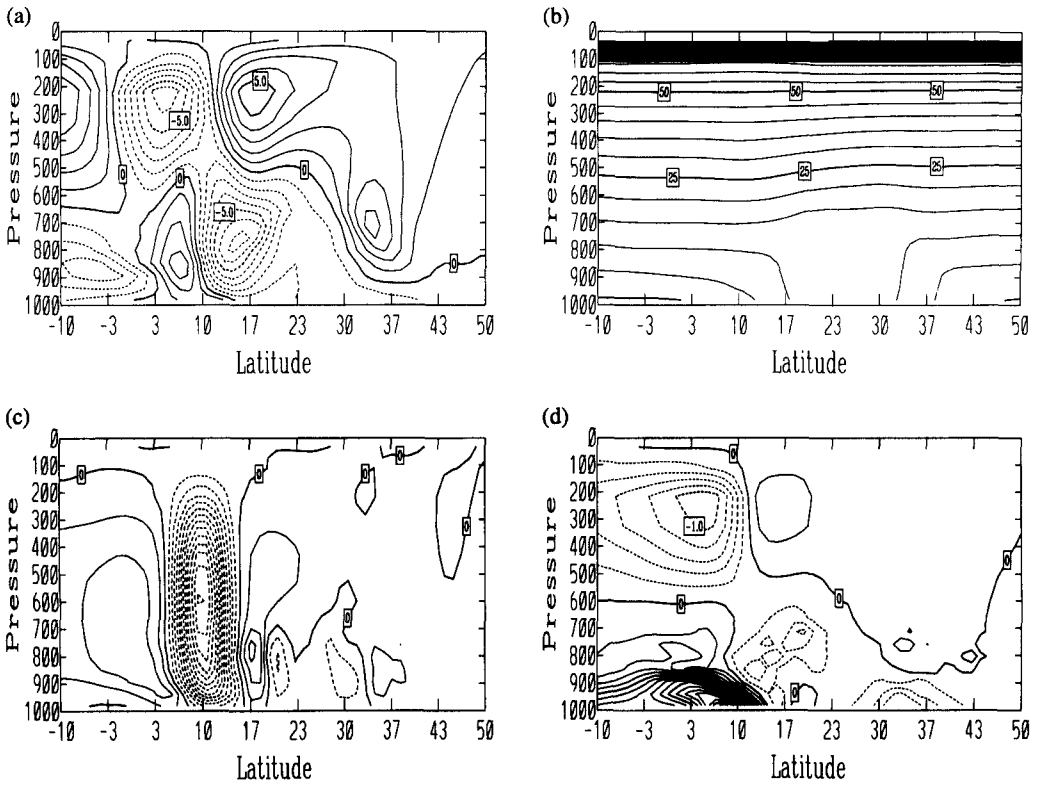

Figure 15. Latitude–pressure (mb) sections of day 0 to day 10 averaged zonal mean fields from the combined heat-low and ITCZ sine-BL run. (a) Zonal wind, contour interval 1 m s^{-1} with dashed contours denoting easterlies; (b) potential temperature minus 300 K, contour interval 5 K; (c) vertical velocity, contour interval 0.2 Pa s^{-1} with dashed lines denoting ascent; (d) meridional wind, contour interval 0.2 m s^{-1} with dashed contours denoting northerlies. See text for details.

with the heat-low heating, both of the resulting secondary circulations will be expected to occur together. This would suggest that the observed AEJ is probably maintained by both types of heating. The AEJ which forms as a response to both types of heating is examined briefly in the next section.

6. Combined heat-low and ITCZ runs

(*a*) *Experimental design*

The initial conditions and model set-up for the experiment presented here are the same as those in the heat-low run discussed in section 4 above, but also include the sine heating at 10°N described in section 5.

(*b*) *Results*

Figure 15 shows 0 to 10-day averaged fields for the combined heating run. The zonal wind distribution clearly has characteristics of both the ITCZ heating and the heat-low runs. As in both of these runs, a lower-tropospheric easterly jet forms around 15°N. In this case the jet has a mean amplitude of 7.5 m s^{-1} compared with 8.6 m s^{-1} and 3.4 m s^{-1} in the heat-low and ITCZ heating (sine-BL) runs respectively, suggesting a greater importance

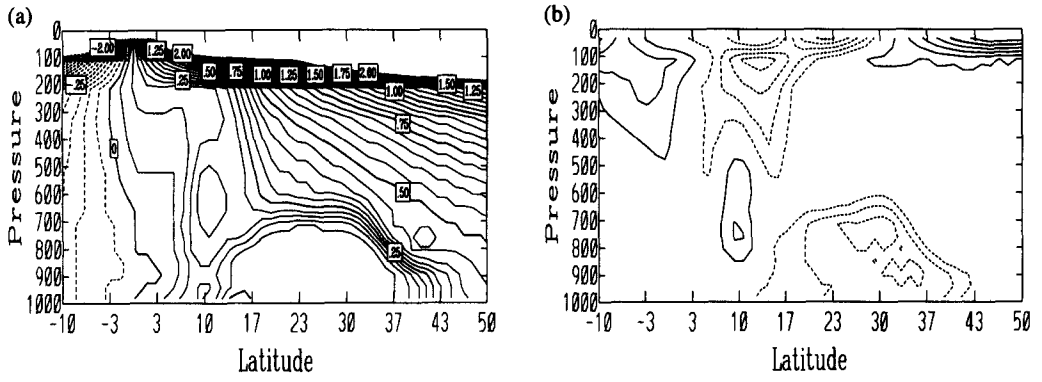

Figure 16. Latitude–pressure (mb) sections of: (a) day 0 to day 10 averaged zonal mean PV from the combined heat-low and ITCZ sine-BL run, contour interval 0.05 PV units with dashed lines denoting negative values; (b) day 10 minus day 0 PV from the same run, contour interval 0.05 PV units with dashed contours denoting PV reduction over the 10-day period. See text for details.

for the heat-low heating. The maximum is located at a height of about 750 mb compared with 700 mb in the heat-low and 800 mb in the ITCZ heating cases. Interestingly, the surface westerly seen on the poleward side of the jet in the heat-low case is not present in the combined case. This may be associated with a weaker south-westerly inflow into the heat-low which results from the low-level convergence at the latitude of the ITCZ heating.

The meridional circulation is dominated by the response to the ITCZ heating by a deep overturning cell. Superimposed on this are the much shallower heat-low cells which are manifested also in the vertical and meridional velocity (v) fields (see Figs. 15(c) and (d)). It is particularly interesting to note that, whereas in the cases of the ITCZ and heat-low heating separately the axis of the $v = 0$ line was vertical, in this combined case it slopes towards the equator in closer agreement with observations (cf. Hastenrath 1991). The slope arises from the superposition of the two meridional circulations induced by the two types of heating.

(*c*) *Potential vorticity*

The 0 to 10-day averaged PV together with the corresponding day 10 minus day 0 difference is shown in Fig. 16. As expected, two important PV anomalies are generated in the region of the AEJ, a negative one in association with the heat-low heating and a positive one mostly in association with the ITCZ heating. These combine to give a marked negative meridional PV gradient in the AEJ maximum, resulting in a flow which bears more resemblence to the ECMWF analyses in Fig. 3 than to the flows seen in the runs with heat-low heating or ITCZ heating alone.

(*d*) *Summary*

As expected, the model simulation which includes both heat-low heating and a representation of ITCZ heating results in a midtropospheric AEJ. The AEJ has characteristics of the AEJs forced by the heat-low and ITCZ heating separately, although for the integrations examined in this study it appears that the heat-low heating is more important. As well as the AEJ, the simulation results in an upper-level easterly jet equatorward of the ITCZ heating and, together with the equatorward sloping confluence line, represents the most realistic simulation examined in this study. It should be realized that the simulation is idealized,

and that there are some unrealistic aspects in the resulting flow; in particular the low-level south-westerly inflow is unrealistically deep. As discussed in section 5 above, this is probably due to the simplified heating profile. Heating profiles could easily be constructed to give more realistic flows, but it is suggested that a more fruitful approach to furthering our understanding of the AEJ would be to consider the role of realistic deep moist convection in more detail.

7. Discussion and conclusions

This study has shown that two diabatically forced meridional circulations are crucial to the maintenance of the AEJ: one associated with surface fluxes and dry convection in the Saharan heat-low region, and one associated with deep moist convection in the ITCZ, equatorward of this. The ITCZ heating has previously been emphasised in the idealized study by Schubert *et al.* (1991). The major conclusion from the present study is that the heat-low heating and circulation, missing in their study, is crucial in maintaining the AEJ and also in setting up the negative meridional PV gradients which characterize the observed AEJ.

In reality, the observed AEJ is both barotropically and baroclinically unstable (Burpee 1972) resulting in easterly waves which grow at the expense of the jet. We may, therefore, view the observed AEJ as resulting from the combination of diabatically forced meridional circulations which maintain it and easterly waves which weaken it.

This view of the AEJ leads us to reflect on the ability GCMs may have in simulating the AEJ. Clearly, if the nature of the diabatic forcing differs between models, for example in association with different parametrizations of deep moist convection or dry convection, then the simulated AEJ is likely to be different. This could result in AEJs with different heights and strengths, which will subsequently affect the easterly waves, possibly resulting in a quite different model climate or forecast. The results shown in section 4(d) above indicate that the rate at which the AEJ is maintained is likely to be particularly sensitive to the boundary layer parametrization. Other aspects not addressed in this study but which must have an effect include: radiation; the establishment of the surface temperature and humidity gradients themselves (e.g. Cook 1999); and sub-gridscale momentum fluxes associated with organized convective systems (e.g. Moncrieff and Klinker 1997; Kershaw and Gregory 1997) which may actually increase the strength of the AEJ.

The view presented here suggests that the nature of the AEJ may vary as the two types of diabatic heating vary, for example either in intensity or in relative position. Indeed, consistent with this, there have been significant changes in the mean AEJ in wet and dry years in the Sahel. Newell and Kidson (1984) showed that the AEJ is stronger and nearer the equator in dry Sahel years and weaker and nearer the poles in wet Sahel years. As discussed in Thorncroft and Hoskins (1994a), this is consistent with thermal wind balance and a surface temperature gradient of the same magnitude but meridionally shifted. A conclusion from the present study is that more will be learnt about how the AEJ is maintained if we consider how the AEJ varies interannually, intraseasonally and even diurnally in association with variations in diabatic forcing and easterly-wave activity.

This paper has shown that the important features of the AEJ can be simulated using a very simple framework in a relatively crude GCM. However, there are clearly limitations to this study which should be addressed in future work. The ITCZ heating here, unlike the heat-low heating, has been prescribed, removing the possibility of feedbacks and interactions with the surface. Future work will include the use of a parametrization of moist convection which will allow the model to develop its own ITCZ heating. Alongside this will be the inclusion of radiative effects. In this more realistic framework, the relationship

between the ITCZ and heat-low circulations can be examined and related more easily to observations and GCM simulations. A further limitation of this study is the assumption of zonal symmetry. The role of growing easterly waves on a realistically diabatically forced AEJ should be investigated in future studies, since the role of easterly waves in damping the AEJ will clearly be a crucial part of the observed AEJ.

The AEJ is a crucial feature of the tropical north African climate. Its maintenance arises through complicated interactions between circulations associated with heat-low and ITCZ heating, together with easterly waves and tropical squall lines. These interactions and how they are represented in GCMs need to be understood more fully if we are to have confidence in forecasts in this region and downstream in the tropical Atlantic. This study offers a simple view of how the AEJ is maintained which will help in future studies of the AEJ.

Acknowledgements

MB is funded by the U.K. Natural Environmental Research Council. CDT acknowledges the Nuffield Foundation for partial funding of this work. We thank ECMWF for making available their analysis data through the British Atmospheric Data Centre.

References

Aspliden, C. I. and Adefolalu, D. 1976 The mean troposphere of West Africa. *J. Appl. Meteorol.*, **15,** 705–716

Betts, A. K. and Miller, M. J. 1986 A new convective adjustment scheme. II: single column tests using GATE wave, Bomex, and arctic air-mass datasets. *Q. J. R. Meteorol. Soc.*, **112,** 693–710

Burpee, R. W. 1972 The origin and structure of easterly waves in the lower troposphere of north Africa. *J. Atmos. Sci.*, **29,** 77–90

Carlson, T. N. and Prospero, J. M. 1972 The large scale movement of Saharan air outbreaks over the northern equatorial Atlantic. *J. Appl. Meteorol.*, **11,** 283–297

Charney, J. G. and Stern, M. E. 1962 On the stability of internal baroclinic jets in a rotating atmosphere. *J. Atmos. Sci.*, **19,** 159–172

Chang, C.-B. 1993 Impact of desert environment on the genesis of African wave disturbances. *J. Atmos. Sci.*, **50,** 2137–2145

Cook, K. 1999 Generation of the African easterly jet and its role in determining west African precipitation. *J. Climate*, in press

Cooper, I. M., Thorpe, A. J. and Bishop, C. H. 1992 The role of diffusive effects on potential vorticity in fronts. *Q. J. R. Meteorol. Soc.*, **118,** 629–647

Fontaine, B., Janicot, S. and Moron, V. 1995 Rainfall anomaly patterns and wind field signals over West Africa in August (1958–1989). *J. Climate*, **8,** 1503–1510

Gill, A. E. 1982 *Atmosphere–ocean dynamics*, Academic Press, London, UK

Hack, J. J., Schubert, W. H., Stevens, D. E. and Kuo, H.-C. 1989 Response of the Hadley circulation to convective forcing in the ITCZ. *J. Atmos. Sci.*, **46,** 2957–2973

Hastenrath, S. 1991 *Climate dynamics of the tropics*. Kluwer Academic Publishers, Dordrecht, The Netherlands

Hoskins, B. J. and Simmons, A. J. 1975 A multi-layer spectral model and the semi-implicit method. *Q. J. R. Meteorol. Soc.*, **101,** 637–655

Hoskins, B. J., McIntyre, M. E. and Robertson, A. W. 1985 On the use and significance of isentropic potential vorticity maps. *Q. J. R. Meteorol. Soc.*, **111,** 877–946

Houze, R. A. and Betts, A. K. 1981 Convection in GATE. *Rev. Geophys. Space Phys.*, **19,** 541–576

Karyampudi, V. M. and Carlson, T. N. 1988 Analysis and numerical simulations of the Saharan air layer and its effect on easterly wave disturbances. *J. Atmos. Sci.*, **45,** 3102–3136

Kershaw, R. and Gregory, D. 1997 Parametrization of momentum transport by convection. I: Theory and cloud modelling results. *Q. J. R. Meteorol. Soc.*, **123,** 1133–1152

Lander, J. and Hoskins, B. J. 1997 Believable scales and parametrizations in a spectral transform model. *Mon. Weather Rev.*, **125,** 292–303

Lindzen, R. S. and Hou, A. Y. 1988 Hadley circulations for zonally averaged heating centered off the equator. *J. Atmos. Sci.*, **45,** 2417–2427

Moncrieff, M. W. and Klinker, E.	1997	Organized convective systems in the tropical western Pacific as a process in general circulation models: A TOGA-COARE case study. *Q. J. R. Meteorol. Soc.*, **123,** 805–828
Newell, R. E. and Kidson, J. W.	1984	African mean wind changes between Sahelian wet and dry periods. *J. Climatol.*, **4,** 27–33
Nicholson, S. E.	1989	African drought: characteristics, causal theories and global teleconnections. Pp. 79–100 in *Understanding climate change. Geophys. Monogr.* 52, IUGG Vol. 7. Eds. A. Berger, R. E. Dickenson and J. W. Kidson. Am. Geophys. Union, Washington DC, USA
Paradis, D., Lafore, J.-P., Redelsperger, J.-L. and Balaju, V.	1995	African easterly waves and convection. Part 1: Linear simulations. *J. Atmos. Sci.*, **52,** 1657–1679
Reed, R. J., Norquist, D. C. and Recker, E. E.	1977	The structure and properties of African wave disturbances as observed during Phase III of GATE. *Mon. Weather Rev.*, **105,** 317–333
Schubert, W. H., Ciesielski, P. E., Stevens, D. E. and Kuo, H.-C.	1991	Potential vorticity modelling of the ITCZ and the Hadley circulation. *J. Atmos. Sci.*, **48,** 1493–1500
Simmons, A. J.	1977	A note on the instability of the African easterly jet. *J. Atmos. Sci.*, **34,** 1670–1674
Thorncroft, C. D.	1995	An idealized study of African easterly waves. III: More realistic basic states. *Q. J. R. Meteorol. Soc.*, **121,** 1589–1614
Thorncroft, C. D. and Hoskins, B. J.	1994a	An idealized study of African easterly waves. I: A linear view. *Q. J. R. Meteorol. Soc.*, **120,** 953–982
	1994b	An idealized study of African easterly waves. II: A nonlinear view. *Q. J. R. Meteorol. Soc.*, **120,** 983–1015
Thorncroft, C. D. and Rowell, D. P.	1998	Interannual variability of African wave activity in a general circulation model. *Int. J. Climatol.*, **18,** 1305–1323
Yanai, M., Esbensen, S. and Chu, J. H.	1973	Determination of bulk properties of tropical cloud clusters from large-scale heat and moisture budgets. *J. Atmos. Sci.*, **30,** 611–627